Sensing actin dynamics through adherens junctions

Indrajyoti Indra, Regina B. Troyanovsky, Lawrence Shapiro[be]*, Barry Honig[bcde]*, Sergey M. Troyanovsky[a]*

[a]Department of Dermatology, Northwestern University, The Feinberg School of Medicine, Chicago, IL 60611
[b]Department of Biochemistry and Molecular Biophysics, [c]Department of Systems Biology, [d]Department of Medicine, and [e]Zuckerman Mind Brain and Behavior Institute, Columbia University, New York, NY 10032, USA.

Running title: Organization of adherens junctions

Key words: Cadherin, actin, adhesion

* Corresponding authors

The Lead Contact:

Dr. Sergey Troyanovsky
Department of Dermatology
Northwestern University
The Feinberg School of Medicine,
303 E. Chicago Ave
Chicago, IL. 60611
Phone: 1-312-503-9275
Email: s-troyanovsky@northwestern.edu

Abstract

We study punctate adherens junctions (pAJs) to determine how short-lived cadherin clusters and relatively stable actin bundles interact despite differences in dynamics. We show that pAJ-linked bundles consist of two distinct regions – the bundle stalk (AJ-BS) and a tip (AJ-BT) positioned between cadherin clusters and the stalk. The tip differs from the stalk in a number of ways: it is devoid of the actin-bundling proteins, calponins and exhibits a much faster F-actin turnover rate. While F-actin in the stalk displays centripetal movement, the F-actin in the tip is immobile. The F-actin turnover in both the tip and stalk is dependent on cadherin cluster stability, which in turn is regulated by F-actin. The close bidirectional coupling between the stability of cadherin and associated F-actin shows how pAJs, and perhaps other AJs, allow cells to sense and coordinate the dynamics of the actin cytoskeleton in neighboring cells – a mechanism we term "dynasensing".

Introduction

Cadherin-mediated adhesion is a defining trait of all metazoans. It is mediated by a transmembrane receptor, a classical cadherin (E-cadherin in many epithelia), which functions in a large multi-protein complex. The unstructured cytoplasmic region of E-cadherin binds directly to β-catenin, which in turn is bound to α-catenin (we denote this as the cadherin-catenin complex, or CCC). The CCC-incorporated α-catenin also interacts with F-actin through its actin-binding domain (Pappas & Rimm, 2006; Harris & Tepass, 2010; Michael & Yap, 2013; Mège & Ishiyama, 2017), providing a bridge between cadherin and the actin cytoskeleton. We recently showed that the extracellular region of punctate adherens junctions (pAJs) consists of dense, paracrystalline nanoclusters formed through *cis* and *trans* interactions of cadherin ectodomains, interspersed with less dense cadherin regions. The nanooclusters in this "mosaic model" assemble and disassemble on a time-scale of seconds in a process that depends on the dynamics of junctional actin (Indra et al., 2018). However, the pAJs are linked to F-actin bundles, which are thought to be among the most stable actin structures. How then can the fast dynamics of cadherin clusters and the much slower turnover of actin bundles be reconciled? Further, the pulling forces the bundles apply on the CCC are essential for both the overall stability of AJs and the tension-dependent recruitment of vinculin and other proteins into AJs (Huveneers & Rooij, 2013; Mège & Ishiyama, 2017). How can these tensile forces be applied between regions with very different dynamical properties? Here we address these questions by studying the spatiotemporal properties of E-cadherin clusters and F-actin bundles in pAJs.

AJs, including pAJs, along with Focal Adhesions (FAs) and tips of lamellipodia, are sites of rapid F-actin polymerization (Vasioukhin et al., 2000; Zhang et al., 2005; Kovacs et al., 2011). However, the polymerization mechanism and the role and fate of polymerized filaments in AJs are poorly understood. In one model, F-actin at AJs is nucleated by the Arp2/3 complex. Direct binding of Arp2/3, to the cytoplasmic tail of E-cadherin (Kovaks et al., 2002), or indirect binding through cortactin (Han et al., 2014), neogenin (Lee et al., 2016), or α-actinin-4 (Tang & Brieher, 2012) have all been suggested as mechanisms for Arp2/3 recruitment into AJs. The Arp2/3-nucleated filaments have been proposed to grow using Ena/VASP proteins (Scott et al., 2006;

Leerberg et al., 2014) and to then be reconfigured from a branched to a bundled array by an N-WASP-dependent mechanism (Kovacs et al., 2011; Brieher & Yap, 2013). This model is challenged, however, by observations that mature AJs are depleted of Arp2/3 (Verma et al., 2004; Hansen et al., 2013) and by proteomics analyses that have failed to identify Arp2/3, neogenin, N-WASP, or α-actinin-4 in association with cadherin tails (Van Itallie et al., 2014; Guo et al., 2014; Li at al., 2019).

There are also uncertainties concerning the configuration and dynamics of F-actin in AJs. Platinum replica Electron Microscopy (EM) identified a pool of branched F-actin at different types of AJs, including at pAJs, of endothelial cells (Efimova & Svitkina, 2018), while other EM studies have suggested that AJs are directly associated with tensile actin bundles (Yonemura et al., 1995; Buckley et al., 2014, Choi et al., 2016; Li at al., 2019). With respect to dynamics, fluorescence recovery after photobleaching (FRAP) and fluorescence loss after photoactivation (FLAP) experiments with MDCK cells showed that AJ-associated F-actin recovers with a half-life of seconds (Yamada et al., 2005), a rate that corresponds to that of the branched F-actin in lamellipodia (Lai et al., 2008; Fritzsche et al., 2013). However, other studies have reported a half-life of about 1 min or even longer (Wu et al., 2014; Cavey et al., 2008; Kovacs et al., 2011), corresponding to that of bundled rather than branched actin (Hotulainen & Lappalainen, 2006).

Here we show that pAJ-associated bundles are composed of two distinct regions: a stable F-actin bundle, which we refer to as the adherens junction bundle stalk (AJ-BS), and a highly dynamic pAJ-proximal region at the tip of this bundle, the adherens junction bundle tip (AJ-BT). The existence of these two connected but distinct actin bundle regions helps to reconcile previous studies, which have alternatively found both branched and dynamic, and bundled and stable F-actin in AJs. Since the dynamical properties of the AJ-BTs are similar to those of CCC clusters, the existence of the tips resolves the issue of a mismatch between bundle and CCC dynamics. Finally, bidirectional coupling between CCC and F-actin dynamics coordinates organization of the actin cytoskeleton in adjacent cells. Our work, therefore, provides a dynamical model of pAJs, which explains how they are able to maintain and synchronize their remarkable flexibility under constant actomyosin stretching. In light of their common protein compositions, this model may be applicable to AJs in general.

Results

AJ-linked actin bundles consist of two distinct regions with differing compositions of actin-binding proteins. Punctate AJs (pAJs) are the most prominent AJs of human squamous carcinoma A431 cells (Indra et al., 2013, 2018), and are identified by E-cadherin staining in Fig 1a. Phalloidin staining showed that they are linked to radial actin bundles of diverse length, which approach each pAJ from two adjacent cells. Their pAJ-attached termini exhibit the strongest phalloidin fluorescence (Fig.1A, arrowheads), perhaps due to overlap of the actin bundles from each cell linked at the junction. The extra-junctional end of the bundle appears to integrate into a dense actin cortical network (Fig 1A).

To better understand the organization of the pAJ-connected bundles, we stained A431 cells for myosin IIA (MyoIIA) and calponin-2 or -3 (Cnn2/3). These proteins have been shown to be abundant in actin bundles in fibroblasts (Tojkander et al., 2012, Ciuba et al., 2018). We found that MyoIIA was typically concentrated several microns away from pAJs (Fig. 1B). By contrast, Cnn2/3 were specifically enriched in the pAJ-connected bundles (Fig. 1C and S1). However, their pAJ-integrated termini were completely devoid of Cnn2/3 (Fig. 1C, arrowhead). Double Cnn3/MyoIIA staining confirmed that calponin-positive pAJ-linked bundles did not incorporate MyoIIA (Fig. 1D).

The absence of Cnn2/3 staining in the pAJ-attached termini suggests that these regions are structurally different from the remaining parts of the bundles, however this observation could also be due to inaccessibility of Cnn2/3 to antibodies at sites of actin-CCC interactions. To distinguish these two possibilities, we expressed recombinant Dendra2-tagged Cnn3 (Cnn3-Dn) in A431 cells. Figures 2A and B show that, consistent with the antibody staining, Cnn3-Dn was efficiently incorporated into the pAJ-linked bundles, but not into their pAJ-integrated termini. Line-scan analysis of fluorescence intensity across the pAJs confirmed that the depressions in Cnn3-Dn incorporation exactly matched the peaks of both F-actin and E-cadherin (Fig. 2E).

We next tested whether major actin cytoskeletal proteins associated with pAJs – vinculin, VASP, mena, and FBLIM1 – were located at the Cnn3-Dn-deficient regions of

the pAJ-linked bundles. Indeed, immunofluorescence microscopy of Cnn3-Dn-expressing cells for these proteins, and line-scan analyses of the resulting images, clearly showed the presence of these proteins in the pAJ-adjacent bundle termini (Fig. 2 C-E and S1). Structured-illumination microscopy (SIM) of E-cadherin, which marks the locations of pAJs, further validated localization of E-cadherin within the Cnn3-Dn-deficient regions of the bundles (Fig. 2F). The average thickness of this region, assessed using 30 independent pAJ images (obtained by SIM or conventional microscopy) was ~ 400 nm (Fig. 2G).

Overall, these results show that a pAJ-linked actin bundle is structurally heterogeneous and encompasses at least two regions (Fig. 2H). The first region, overlaps with the CCC at the light microscopy resolution level. It exhibits highest F-actin deposition, is enriched with VASP, mena, FBLIM1, and vinculin, and is devoid of Cnn2/3. We denote this region as the bundle tip (AJ-BT) which, given the 400 nm total length of the Cnn2/3-deficient area, has a length in each cell on the order 200 nm. The second region corresponds to the bundle stalk (AJ-BS), which is enriched with Cnn2/3. The distal end of AJ-BSs interacts with the AJ-BT while the opposite end is integrated into the contractile actomyosin network, which ultimately transmits the mechanical forces into this system.

F-actins in AJ-BSs and AJ-BTs have different dynamical properties. The relatively large size of the tip region allows it to be analyzed using conventional light microscopy. To this end, we produced A431 cells that stably express a photoactivatable form of actin, mCH_{PA}-actin. Previous studies have shown that actin tagged with fluorescent proteins assembles into filaments and can serve as an excellent probe of F-actin dynamics (Yamada et al., 2005; Tojkander et al., 2015). Indeed, double immunostaining of the transfected cells for mCH_{PA}-actin and phalloidin showed that the actin bundles of these cells recruited the recombinant actin (Fig. 3A). Furthermore, similar to the untagged actin in the control cells, mCH_{PA} -actin produced bright plaques at sites of E-cadherin-based pAJs (Fig. 3B). In order to specifically photoactivate mCH_{PA} fluorescence at bundle tips or at bundle stalks, we developed a "pAJ-actin dynamics" assay in which the mCH_{PA}-actin cells were co-cultured with EcGFP-expressing A431 counterparts (see Fig. 3C).

These mCH$_{PA}$-actin/EcGFP co-cultures allowed us to study actin dynamics in mixed pAJs, one half of which was highlighted by EcGFP with the other half expressing the "dark" mCH$_{PA}$-actin.

First, we photoactivated mCH$_{PA}$ precisely at pAJ sites using the maximum focused laser beam (Fig. 3C, AJ-BT, movie S1). Time lapse imaging showed that at this position, the spot of red mCH$_{PA}$-derived fluorescence (its diameter encompassed ~4-5 pixels, or 440-550 nm) exhibited a relatively short lifetime, with the half-life of fluorescence decay ~ 20 sec, with low variation between experiments (Fig. 3D and E). The photoactivated spot, usually trackable for up to 1 min, was immobile and tightly associated with the selected pAJ during the entire observation period (Fig. 3F). To probe actin dynamics in the AJ-BSs, we targeted the laser beam to sites located about a half micron from the pAJ toward the center of the dark cell (Fig. 3C, AJ- BS, movie S2). Remarkably, at these sites the decay of photoactivated spots was significantly slower and furthermore, in most cases the spots showed retrograde movements (Fig. 3F). Both of these features, the retrograde movement (median ~ 400 nm/min) and the rate of fluorescent decay (median t1/2 ~ 50 sec) significantly varied between individual junctions (Fig. 3E, F). To ensure that the F-actin dynamic features were specific for the selected spots along pAJ-linked bundles, we performed control experiments, which targeted sites near to, but outside of, the pAJs. At these locations, where junctional actin is not present (Fig. 3C, D, movie S3), the half-life of the resulting red fluorescence decay (~ 10 sec) was significantly faster than in AJ-BTs.

Taken together, the pAJ-actin dynamics assay confirmed the compound architecture of the pAJ-linked actin bundles. Their AJ-BTs appear to consist of short-lived F-actin whose turnover rate of about 20 seconds is similar to that of lamellopodium actin (Fritzsche et al., 2013; Lai et al., 2008). By contrast, F-actin in AJ-BSs exhibited characteristics more similar to those in dorsal actin bundles linked to FAs, which display centripetal flow with an average half-life of ~ 2 min (Hotulainen & Lappalainen, 2006; Tojkander et al., 2015). While we cannot exclude the possibility that a small pool of AJ-BT-linked F-actin eventually moves into the AJ-BS, the bulk of the AJ-BT F-actin was immobile and tightly coupled with the CCC in pAJs.

Cadherin cluster stability regulates F-Actin turnover in AJ-BTs and AJ-BSs. The fast turnover of AJ-BT F-actin suggests that the assembly-disassembly of both F-actin and cadherin clusters is tightly coupled. This idea is supported by previous observations that stabilization of F-actin by Jasplakinolide prolonged the lifetime of cadherin clusters in pAJs (Indra et al., 2018). Does the turnover of F-actin in AJ-BTs depend on the stability of cadherin clusters? To answer this question, we studied how different manipulations known to affect cadherin cluster dynamics influence that of F-actin. The green fluorescence in one half of pAJs in our mCH_{PA}-actin/EcGFP co-cultures allowed us to use FRAP technique to determine the dynamical properties of cadherin in pAJs. While FRAP significantly underestimates the rate of cadherin cluster assembly and disassembly due to local reincorporation of cadherin into new clusters (Indra et al., 2018), this approach is useful for the general assessment of cadherin cluster stability. First, we expose the co-cultures to hypertonic shock, which we have shown to dramatically reduce cadherin dynamics in pAJs (Troyanovsky et al., 2006). Indeed, after 10 min in hypertonic sucrose media, the recovery of EcGFP fluorescence in pAJs as well as the decay of mCH_{PA}-actin photoactivated fluorescence in AJ-BTs was nearly completely stalled (Fig. 4A, B). Interestingly, the mCH_{PA}-actin turnover in AJ-BSs as well as its retrograde flow were also blocked (Fig. 4B, C).

Since hypertonic shock abolished pAJ disassembly through relatively indirect and still unknown mechanisms, we chose to modify cadherin cluster stability directly using specific point mutations that effect cadherin ectodomain *trans* and *cis* interactions. Specifically, in the mCH_{PA}-actin/EcGFP co-culture, we replaced the EcGFP cells with cells expressing mutant EcGFP. The first, involving the P5A mutant that dramatically strengthens the K_D of cadherin *trans*-bonds, from ~100 μM to 3 μM (Vendome et al., 2011), and thus increases cluster stability. Notably, since P5A forms "extra" hydrogen bonds in *trans* with distal β-strand residues, the strengthening effect of this mutation should also be observed when binding to wild-type E-cadherin (Vendome et al., 2011). The second mutant targets the *cis*-binding interface of E-cadherin and destabilizes pAJs by disrupting the paracrystalline lattice formed by cadherin ectodomains (Harrison et al., 2011; Strale et al., 2015).

We first performed a set of control experiments in order to confirm that in the mixed pAJs in our co-cultures, the P5A-EcGFP mutant would indeed decrease, and the EcGFP cis-mutant would increase, the turnover rate of the intact E-cadherin present in the mCH_{PA}-actin-expressing cells. We showed that both mutants established mixed pAJs with mCH_{PA}-actin-expressing cells and that these mixed pAJs were linked to the mCH_{PA}-actin bundles (Fig. 4D). Then, using a FRAP assay with the mutant-expressing cells in homogeneous cultures and in co-cultures with mCH_{PA}-actin-expressing cells, we verified that both mutants changed EcGFP turnover rates as expected. Indeed, fluorescence recovery curves (Fig. 4E) showed that the P5A mutation significantly reduced, while the *cis* mutation, by contrast, increased, the pAJ cadherin turnover rate in both the mixed and homogeneous pAJs. The P5A mutant likely stabilizes mixed pAJs through enhanced *trans* interactions with wild-type E-cadherin, whereas the *cis* mutant destabilizes pAJs likely by disrupting one half of the E-cadherin lattice, thus disrupting the other half.

Finally, we confirmed that turnover of the wild-type E-cadherin on one half of pAJs matched that of the mutant E-cadherin present on the opposite side of the same pAJ. To show this, we co-cultured the mutant-expressing cells with A431 cells expressing mCH-tagged E-cadherin (EcmCH). Both, GFP and mCH fluorophores in the hetero-chromatic pAJs were simultaneously bleached and recovery of their fluorescence simultaneously monitored by time-lapse microscopy (Fig. S2). This two-color FRAP experiment revealed that E-cadherin turnover rates were indeed balanced in both sides of AJs, consistent with previously published data showing that cadherin turnover rates are closely correlated in two halves of the same junction (de Beco et al., 2015).

These observations confirmed that the replacement of EcGFP with P5A-EcGFP or with cis-EcGFP, respectively, either slowed or increased wt E-cadherin turnover in the mCH_{PA}-actin-expressing cells connected through mixed pAJs in our co-cultures. Next, using our pAJ-actin dynamics assay, we determined actin turnover rates in these junctions. The results clearly showed that AJ-BTs from the pAJs for which the opposite half incorporated the P5A-EcGFP mutant exhibited a significant increase in the lifetime of mCH_{PA} red fluorescence ($t1/2 \sim 40$ sec). By contrast, mCH_{PA} fluorescence in AJ-BTs for which pAJs contacted cis-EcGFP-expressing cells had much shorter lifetimes, with $t1/2$ of just few seconds (Fig. 4F). Surprisingly, both mutations correspondingly changed

the F-actin turnover not only in the AJ-BTs, but also in the AJ-BSs (Fig. 4F). Finally, the centripetal flow of the red spot photoactivated at the AJ-BSs was nearly completely stalled in the cells connected to P5A-EcGFP but, in contrast, increased in *cis*-mutant EcGFP co-cultures (Fig. 4G).

F-actin dynamics are coordinated between adjacent cells. Our previously reported data suggest that F-actin turnover regulates the rate of cadherin cluster assembly and disassembly (Indra et al., 2018). Here we have demonstrated that the inverse phenomenon also takes place: cadherin cluster dynamics control the rate of F-actin turnover in pAJ-linked bundles. These observations imply that F-actin polymerization-depolymerization rates in both halves of a pAJ are coordinated. To test this hypothesis we assessed whether, in the mCH_{PA}-actin/EcGFP co-culture, F-actin stabilization in the EcGFP expressing cells would stabilize F-actin in the adjacent mCH_{PA}-actin-expressing cells.

To stabilize F-actin in the EcGFP-expressing cells, we knocked out a key actin depolymerizing factor, cofilin 1 (Cfl1), using a CRISPR/Cas9 approach. The lack of Cfl1 has been shown to reduce the F-actin depolymerization rate of the branched actin network of different types of cells, but does not abolish AJs (Lappalainen & Drubin, 1997; Hotulainen et al., 2005; Iwasa & Mullins, 2007; Vitriol et al., 2013; Wang et al., 2016). As has been shown for other cell types, Cfl1 knockout in the EcGFP-expressing A431 cells resulted in cell shape flattening, which may be caused by unbalanced actin polymerization in cell lamellopodia. Despite these changes, as has been observed previously (Chu et al., 2012; Wang et al., 2016), the Cfl1-KO cells retained their pAJs (Fig. 5A) and general actin bundle organization, as revealed by phalloidin and anti-Cnn3 staining (Fig. 5B, C). As expected from our previous experiments with Jasplakinolide (Indra et al., 2018), the FRAP assay showed a significant stabilization of E-cadherin in AJs upon Cfl1 knockout (Fig. 5D, homogeneous pAJ).

EcGFP in the Cfl1-KO cells showed nearly the same turnover rate in the co-culture with mCH_{PA}-actin-expressing cells as in the homogeneous culture (Fig. 5D). As expected from this observation, photoactivation of mCH_{PA}-actin in such co-cultures showed that the Cfl1-KO EcGFP-expressing cells significantly stabilized actin in both

AJ-BTs and AJ-BSs in adjacent cells (Fig. 5D). Together, these experiments suggest that the reduction of F-actin dynamics induced by Cfl1-KO in EcGFP-expressing cells was transduced into the neighboring cells through reduction of cadherin turnover in AJs.

pAJs are enriched with factors driving dynamics of the branched actin cytoskeleton. To further shed light on the organization of pAJ-associated actin filaments and mechanisms of their fast dynamics, we stained A431-EcGFP cells for proteins known to bind and regulate the dynamics of branched actin filaments. First, we extended our examination of Cfl1. This protein transiently targets and severs actin filaments in collaboration with another protein, Aip1 (Bravo-Cordero et al., 3013; Ono, 2018). While, as observed for other cell types (Abe et al., 1993; Munsie et al., 2012), Cfl1 was mostly cytosolic in A431 cells, many of the well-isolated pAJs exhibited Cfl1-specific puncta (Fig. 6A). Line-scan analyses confirmed close spatial association between pAJs and such Cfl1 puncta (Fig. 6A, E). It has been shown that in absence of Aip1, Cfl1 binds to but does not sever filaments, leading to accumulation of Cfl1-bound F-actin (Kato et al., 2008); we exploited this observation to clearly identify the pool of Cfl1-targetted actin filaments in Aip1 knock-out A431-EcGFP cells. As shown in Figure 6B, these cells exhibited numerous Cfl1-decorated cortical filaments, which were especially prominent in pAJs (Fig. 6B). The strong enrichment of Cfl1 in pAJ-linked filaments, together with the dramatic reduction of actin and E-cadherin turnover in pAJs upon Cfl1 knockout, strongly suggests that Cfl1 plays a direct and critical role in F-actin homeostasis in pAJs.

Next we studied localization of Arp2/3, a key protein complex involved in organization and dynamics of the branched actin cytoskeleton. As highlighted in the Introduction, there are strong uncertainties about the mechanisms of Arp2/3 recruitment into AJs and even about its presence in mature AJs (Verma et al., 2004; Hansen et al., 2013). This uncertainty stems in part from the fact that Arp2/3 is abundant in the cell cortex and is especially enriched in cell-cell contact areas. To reduce cytosolic pools of Arp2/3, we fixed cells in cytoskeleton-preserving buffer in the presence of Triton X-100. Figures 6C and 6D show that Arp2/3 and its cofactor, cortactin, were highly concentrated in the cell-cell contact regions. In contrast to Cfl1, for which peak intensity usually corresponded to that of E-cadherin, Arp2/3 and cortactin were located in relatively large

zones encompassing the pAJs (Fig. 6D). These results suggest that Arp2/3, in agreement with proteomics data, might not be specifically targeted into mature pAJs. Instead Arp2/3 might be involved in formation and dynamics of the entire actin cortex of the lateral membranes in which the AJ-BTs are integrated. More work is needed to understand whether Arp2/3 plays a specific role in generation and dynamics of CCC-coupled F-actin.

Discussion

In this work we show that pAJ-linked actin bundles consist of two distinct regions: a bundle stalk, the AJ-BS, which connects the bundle to the actomyosin cytoskeleton and a bundle tip, the AJ-BT, which serves as a joint between the relatively stable stalk and the highly dynamic adhesive region of pAJs. Our FLAP experiments show that the half-life of F-actin in AJ-BTs is ~20 sec as compared to ~1 min in AJ-BSs. Time-lapse recordings of these adjacent F-actin regions suggest that they are generated by distinct F-actin assembly pathways since mCH_{PA}-actin activated in AJ-BTs does not translocate into the AJ-BS, but remains associated with corresponding pAJs over its entire lifetime. The F-actin in the AJ-BS, by contrast, is not immobile but flows rearward.

These differences in dynamics may reflect the striking structural difference between these two bundle compartments. The AJ-BS apparently consists of parallel actin filaments since it is enriched with the prominent actin bundling proteins calponin-2 and calponin-3. The AJ-BT lacks these bundling proteins, but instead is enriched with proteins involved in actin dynamics, such as mena and VASP. The F-actin depolymerization factor, Cfl1, which plays key role in dynamics of the branched actin networks (Chan et al., 2009; Bravo-Cordero et al., 2013), is also colocalized with AJ-BTs. The role of this factor in AJ-BT dynamics is supported by the dramatic stabilization of these structures upon Cfl1 knockout. AJ-BTs are integrated into the cell-cell contact areas enriched with Arp2/3, known to play a role in nucleation of branched actin networks. This dual organization of pAJ-linked actin bundles is consistent with a recent platinum replica EM study of endothelial AJs, which shows that bundles of parallel actin filaments are linked to a VE-cadherin-rich zone through a ~200-300 nm thick branched actin network (Efimova & Svitkina, 2018).

Our study also reveals that during its entire lifespan F-actin photoactivated in AJ-BTs associates with pAJs. This observation is important since it suggests that assembly-disassembly cycles of F-actin in AJ-BTs are coupled with those of cadherin clusters to which they are linked via α-catenin. This idea is further reinforced by the observed bidirectional relationship between F-actin and cadherin turnover. In all cases when F-actin was stabilized, E-cadherin clusters also showed increased stability. Our study provides two examples of this relationship: knockout of the F-actin depolymerization

factor Cfl1 and osmotic shock all simultaneously increased the lifetime and immobile fraction of both E-cadherin and F-actin in AJ-BTs. These observations are in line with previous data showing that F-actin stabilization by Jasplakinolide increases stability of E-cadherin clusters in AJs (Indra et al., 2018). Here we have shown that the inverse is also true: increases or decreases in the lifetime of E-cadherin clusters in pAJs induced by mutant E-cadherins correspondingly changed F-actin lifetimes.

The precise spatiotemporal organization of F-actin in AJ-BTs and the mechanisms responsible for the close coupling between actin and cadherin cluster turnover are still unclear and are important avenues for future research. Figure 7 presents a very general schematic model, based on the results published here and previously (Indra et al., 2018; Efimova & Svitkina, 2018), as to how F-actin and cadherin cluster dynamics are coupled and coordinated. The figure illustrates how parallel and stable actin filaments of the AJ-BS interact with apparently branched and dynamic actin filaments in the AJ-BT, which in turn, interact with the CCC. Our results strongly suggest that each cadherin nanocluster associates with its own "tangle" of the branched F-actin network. The top panel depicts two cadherin nanoclusters linked to two such tangles that are separated by a region of lower cadherin and actin density. In the bottom panel, these two tangles and associated CCC clusters depolymerize and a new tangle linked to a new cadherin cluster is formed. The transition between the structures shown in the two panels involves the rearrangement of cadherin clusters that continuously dissociate and reform in pAJs as a result of two coupled processes which are each cooperative: an extracellular process involving *cis* and *trans* cadherin interactions (Harrison et al., 2011; Strale et al., 2015) and an intracellular process involving α-catenin binding to F-actin (Hansen et al., 2013; Buckley et al., 2014; Chen et al., 2015). It is possible that Arp2/3 and Cfl1 play key roles in this process. Importantly, new cadherin clusters continuously reutilize E-cadherin of the disassembled clusters, which results in underestimation of cadherin turnover rate by FRAP or FLAP assays (Indra et al., 2018). By contrast, the requirement for ADP-ATP exchange impedes the immediate reuse of the G-actin released from the disassembled F-actin tangles. This difference in assembly mechanisms could be a major reason for significant differences in a half lives of E-cadherin and AJ-BT actin in pAJs, (~5 min and ~ 20 sec, respectively).

Close coupling between cadherin clusters and F-actin in AJ-BTs resolves the question highlighted in the Introduction about the apparent mismatch between cadherin and F-actin turnovers in pAJs. Furthermore, it explains how tensile actomyosin-based forces conducted by the AJ-BS can be applied to the "fluid" cadherin-based adhesive interface of pAJs: at each given moment the interface contains many cadherin adhesive clusters that are each linked to the tensile AJ-BS through their own tangles of F-actin. A new question now arises, however, as our findings show that there is indeed a mismatch, but it is between AJ-BT and AJ-BS F-actin dynamics. This mismatch suggests that the AJ-BS/AJ-BT interface has novel properties, which are yet to be fully understood. We speculate that the AJ-BS/AJ-BT interface may correspond to a two-sided platform, which continuously produces short-lived tangles of branched F-actin on its AJ-BT side and stable parallel filaments on the opposite, AJ-BS side. Indeed, the centripetal flow we observed for photoactivated actin in AJ-BS suggests active actin polymerization within the bundle, including at the AJ-BS/AJ-BT interface. This polymerization, together with pulling forces generated by MyoIIA, could underlie the rearward treadmilling along bundles we observed for photoactivated AJ-BS actin spots. Interestingly, both the kinetics of the loss of this spot fluorescence and its treadmilling speed depend on E-cadherin stability in pAJs. This dependence suggests that homeostasis of F-actin in the AJ-BS and AJ-BTs as well as that of cadherin clusters are interconnected, despite the fact that, as indicated above, F-actin in AJ-BT and AJ-BS use different actin polymerization pathways. This complex organization of pAJs may also be relevant to other types of AJs. Indeed, branched actin interconnecting CCCs with actin bundles have been detected in linear AJs (Efimova & Svitkina, 2018), and increased rearward treadmilling induced by the cis E-cadherin mutant was noted in actin bundles connected to E-cadherin coated substrates (Strale et al., 2015).

Our findings reveal remarkable similarities between AJ-BSs and the dorsal actin bundles linked to FAs. Both types of bundles are enriched with calponins-2 and -3, but not with MyoIIA (Tojkander et al., 2012). They both include relatively stable F-actin, which continuously polymerizes at the junction-attached end of the bundle and then flows rearward. In the case of FAs, the most active polymerization occurs at the interface between the bundle and integrin-associated proteins (Hotulainen & Lappalainen, 2006).

The opposite ends of these bundles, distal from junctions, are interconnected with the actomyosin contractile system. Analogous to our observations with pAJs, all proteins within FAs turn over rapidly despite the overall morphological stability of the FA (reviewed in Geiger et al., 2009; Case& Waterman, 2015). Moreover, the adhesive regions of FAs consist of small integrin clusters (reviewed in Changede & Sheetz, 2017), while those in pAJs consist of small cadherin clusters (Indra et al., 2018). Nevertheless, specialized connecting structures analogous to AJ-BTs have not been detected for FAs. It should be noted, however, that F-actin directly associated with FAs is enriched with the same proteins as F-actin in AJ-BTs: vinculin, mena, VASP, and FBLIM1 among them.

Both AJs and FAs function as key force transmission complexes of cells. They sense tensile forces exerted on cells and instruct cell behavior in accordance with these forces (reviewed in Geiger et al., 2009; Huveneers & Rooij, 2013; Mège & Ishiyama, 2017; Yap et al., 2018). However our results suggest that AJs sense attached cells using a unique mechanism, which allows them to be rigid enough to transmit force while fluid enough to facilitate cell migration. Specifically, the half of a pAJ in one cell senses the dynamics of cadherin and F-actin in the half of the pAJ in the adjacent cell thus allowing for synchronization of their dynamics. Potentially, this sensing, which we term "dynasensing", may play critical role in morphogenesis, for example, by accelerating the movement of particular types of cells within a stable epithelial sheet. The mechanism suggests how mobile cells could instruct stationary cells to form flexible AJs, which, rather than impeding cell motion, could facilitate movement. Such sensing and synchronization of junction dynamics could thus facilitate cell intercalating events during normal morphogenesis or the invasion of malignant cells.

In conclusion, we show that pAJ-linked actin bundles consist of a stable stalk and a dynamic tip. In the tip, short-lived F-actin polymerization-depolymerization cycles are tightly coupled with assembly-disassembly cycles of cadherin clusters. The coupling between E-cadherin and actin turnover allows pAJs to function not only as flexible mechanosensing connectors between the actin cytoskeleton of neighboring cells, but also as sensors and synchronizers of their cytoskeletal dynamics.

Acknowledgments

Sequencing, Flow Cytometry, and confocal microscopy were performed at the Northwestern University Genetic, Flow Cytometry, and Advanced Microscopy Centers. The authors declare no competing financial interests. The work was supported by grants from the National Institutes of Health: AR044016 and AR070166 (to S.T.), GM118584 (to L.S.) and National Science Foundation Grant MCB-1914542 (to B.H.).

Author contributions

I.I., R.T. and S.T. conducted the experiments, collected and analyzed the data, and prepared the figures. L.S., B.H. and S.T. designed the experiments and wrote the manuscript. S.T. supervised the study.

Figure Legends

Figure 1. Organization of pAJ-linked actin bundles in A431 cells. Projections of all x-y optical slices of A431 cells stained for: **(A)** E-cadherin (Ecad, red) and F-actin (actin, green); **(B)** E-cadherin (green), F-actin (red), and myosin IIA (myosin IIA, blue); **(C)** E-cadherin (green), actin, and calponin-3 (Cnn3); **(D)** Calponin-3 (green) and myosin IIA (red). Bar, 10 μm. The zoomed areas (indicated by dashed boxes) are presented on right panel. Bar, 5 μm. Group of pAJs in a left panel in (A) is further magnified in the inset. Arrowheads in (A-C) indicate Adherens Junction Bundle Tips (AJ-BT), which are enriched with F-actin and E-cadherin, but are devoid of myosin IIA and Cnn3. Arrowhead in (D) shows that myosin IIA is not integrated into a Cnn3-positive pAJ-linked bundle.

Figure 2. F-actin in AJBT regions of pAJ-linked bundles associates with a distinct set of actin-binding proteins. (A-D) Projections of all x-y optical slices of Cnn3-Dn-expressing A431 cells imaged for Dendra2 fluorescence (green, Cnn3-Dn) and stained for: **(A)** E-cadherin; **(B)** actin; **(C)** vinculin (Vcl); **(D)** mena (mena). Bar, 10 μm. The zoomed areas (indicated by dashed boxes in Cnn3-Dn images) are presented at the bottom. Bar, 5 μm. Arrowheads indicate the gaps in Cnn3-Dn distribution along pAJ-linked bundles that are precisely matched by the antibody staining. **(E)** Line-scan analysis of the selected pAJs for distribution of Cnn3-Dn (green) and the indicated pAJ-associated proteins revealed by specific antibodies (red). **(F)** N-SIM of Cnn3-Dn-expressing A431 cells double stained for Dendra2 (green, Cnn3) and E-cadherin (red). Arrowhead indicates AJ-BT region. Bar, 10 μm. The zoomed areas (indicated by dashed boxes in Cnn3-Dn images) are presented at the bottom. Bar, 5 μm. **(G)** The thickness of the Cnn3-Dn-deficient regions measured for 15 independent pAJs on N-SIM and on confocal images. **(H)** Schematic representation of pAJ-linked bundles. Each bundle appears to consist of at least two regions. The first region, AJ-BT (AJ-BT), which is Cnn2/3-deficient (CNN2/3-) directly contacts the cadherin-catenin complex (CCC). The second, Cnn2/3-positive (CNN2/3+) region, AJ-BS, is attached to AJ-BT and interconnects the AJs with the actomyosin cytoskeleton.

Figure 3. Dynamics of F-actin in AJ-BTs and in AJ-BSs. (A-B) Maximum projection view of A431 cells stably expressing mCH$_{PA}$-actin stained for: **(A)** actin using Phalloidin (actin, green) and mCH$_{PA}$-actin using anti-mCH antibody (mCH, red); **(B)** E-cadherin (Ecad, green) and mCH$_{PA}$-actin (red). Bar (in A and B), 10 μm. The zoomed areas (indicated by dashed boxes in actin and Ecad images) are presented at the bottom. Bar, 5 μm. **(C)** Time-lapse series of mCH$_{PA}$-actin photoactivated in the co-cultures of mCH$_{PA}$-actin- and EcGFP-expressing cells. The series were taken in green and red imaging channels: green channel detects EcGFP, while red channel detects only background fluorescence before photoactivation. The full-screen images (left) show groups of cells just before photoacivation. Bar, 10 μm. The time-lapse frames of the boxed areas are zoomed at the right panels and the arrowheads show the selected pAJs before photoactivation (-1), immediately after (0) and then at particular following time points (exact time is indicated in sec). Red fluorescence of mCH$_{PA}$-actin was activated in diffraction-limited spots (~ 500 nm in diameter) in three different locations: exactly at sites of EcGFP-tagged pAJs (AJ-BT); about 0.5 μk toward the center of the dark cell (AJ-BS), or at the pAJ lateral sides (Lateral to AJ). Bars, Bar, 5 μm. **(D)** Kinetics of decay of mCH$_{PA}$-actin photoactivated in AJ-BT, AJ-BS, and lateral to pAJ (n = 10). **(E)** Parameters for mCH$_{PA}$-actin fluorescence decay assessed from curves presented in (D). **(F)** Displacement of individual photoactivated spots of actin over 1 min (n=10).

Figure 4. Cadherin regulates F-actin turnover in pAJ-linked bundles. **(A)** FRAP of EcGFP in pAJs after 10 min in hypertonic sucrose media. **(B)** Decay of mCH$_{PA}$-actin photoactivated in AJ-BT (Actin-AJ-BT) or in AJ-BS (Actin-AJ-BS). **(C)** Displacements of the photoactivated spot as in Fig. 3F. **(D)** Maximum projection view of three different co-cultures of A431 cells. One of sublines stably expresses mCH$_{PA}$-actin, which is visualized by anti-mCH staining (mCH, red). These cells form mixed pAJs with cells stably expressing EcGFP (GFP, green), or its mutants, *cis*-mutant EcGFP (cis-GFP) and P5A-EcGFP (P5A-GFP). Bar, 10 μm. The zoomed areas (indicated by dashed boxes in green images) are presented on the right panel. Bar, 5 μm. **(E)** FRAP of pAJs in cells expressing EcGFP or its mutants P5A-EcGFP or *cis*-mutant EcGFP (n=15). FRAP was

performed either in homogeneous cultures of corresponding cells (Homogeneous pAJ) or in co-cultures with "dark" mCH_{PA}-actin-expressing A431 cells. In the latter case the pAJs located between two types of cells were studies. **(F)** Decay of mCH_{PA}-actin spots photoactivated in pAJs (Actin-AJ-BT) or in bundles (Actin-AJ-BS) in co-cultures with EcGFP or its mutants. Right panel shows parameters of corresponding decays. **(G)** Displacements of the photoactivated spots as in (C).

Figure 5. Knockout of Cfl1 affects actin dynamics in the neighboring wt cells. (A-C) Maximum projection view of control A431-EcGFP cells (A431-EcGFP) or after Cfl1-KO (A431-EcGFP-Cfl1-KO). Cells were imaged for GFP (EcGFP) and for: **(A)** Cfl1 (Cfl, red); **(B)** actin (actin, red); **(C)** Cnn-3 (Cnn3, red). Bar, 10 μm. The zoomed areas (indicated by dashed boxes in EcGFP images) are presented in the insets (A) or at the bottom (B, C). Bar, 5 μm. **(D)** FRAP of pAJs in control and in Cfl1-KO A431-EcGFP cells (n=15). FRAP was performed either in homogeneous cultures of corresponding cells (Homogeneous pAJ) or in co-cultures with "dark" mCH_{PA}-expressing A431 cells. In the latter case the pAJ between dark cells and cells expressing EcGFP were studied. The corresponding FRAP parameters are shown in the bottom. **(E)** Decay of mCH_{PA}-actin spots photoactivated in pAJs (Actin-AJ-BT) or in bundle stalks (Actin-AJ-BS) in mCH_{PA}-actin expressing cells co-cultured with A431-EcGFP or A431-EcGFP-Cfl1-KO cells. The corresponding parameters of mCH_{PA}-actin turnover are shown at the bottom panel.

Figure 6. Subcellular localization of proteins involved in branched actin dynamics: Cfl1, Arp2/3 and cortactin. **(A-D)** Projections of all x-y optical slices of A431-EcGFP cells (**A**, **C**, **D**) and A431-EcGFP-Aip1-KO cells (**B**) imaged for GFP fluorescence (green, EcGFP) and stained for Cfl1 (Cfl), Aip1 (Aip), Arp2/3 (Arp2/3), and cortactin (CTTN). Bar, 10 μm. The zoomed areas (indicated by dashed boxes in EcGFP images) are presented at the bottom or in the insets (for anti-Aip staining in A). Arrowheads indicate pAJs, which exhibit clear colocalization with the antibody-stained proteins. Arrows marked pAJs, which colocalization with the stained protein is unclear because of high nearby fluorescence. Bar, 5 μm. **(E)** Line-scan analysis of the pAJs (selected by

arrowheads in A-D) for distribution of EcGFP (green) and the indicated pAJ-associated proteins (red). In the case of Arp2/3 and cortactin two line-scans are shown, one for arrowhead and another arrow marked pAJs.

Figure 7. Schematic model of coupling between F-actin and cadherin in pAJs. A hypothetical cross-section of a pAJ is shown. Blue parallel lines represent the actin bundle stalk (AJ-BS) apparently consisting of parallel actin filaments of the same polarity. The stalk is terminated with the bundle tip (AJ-BT) shown by red intersecting lines, which in turn interact with the cadherin-catenin complexes (green, CCC). Initially (the top image) the bundle tip consists of two cadherin clusters (1 and 2), formed in association with corresponding tangles of branched F-actin . In the bottom panel, these tangles and associated clusters are disassembled and a new CCC cluster (3) and a corresponding new actin tangle are assembled. The new cluster recruits only few new cadherin molecules (yellow), but the new tangle is built entirely from newly delivered G-actin (magenta). The AJ-BT/AJ-BS interface is positioned to play a key role in dynamics and/or organization of both AJ-BT and AJ-BS.

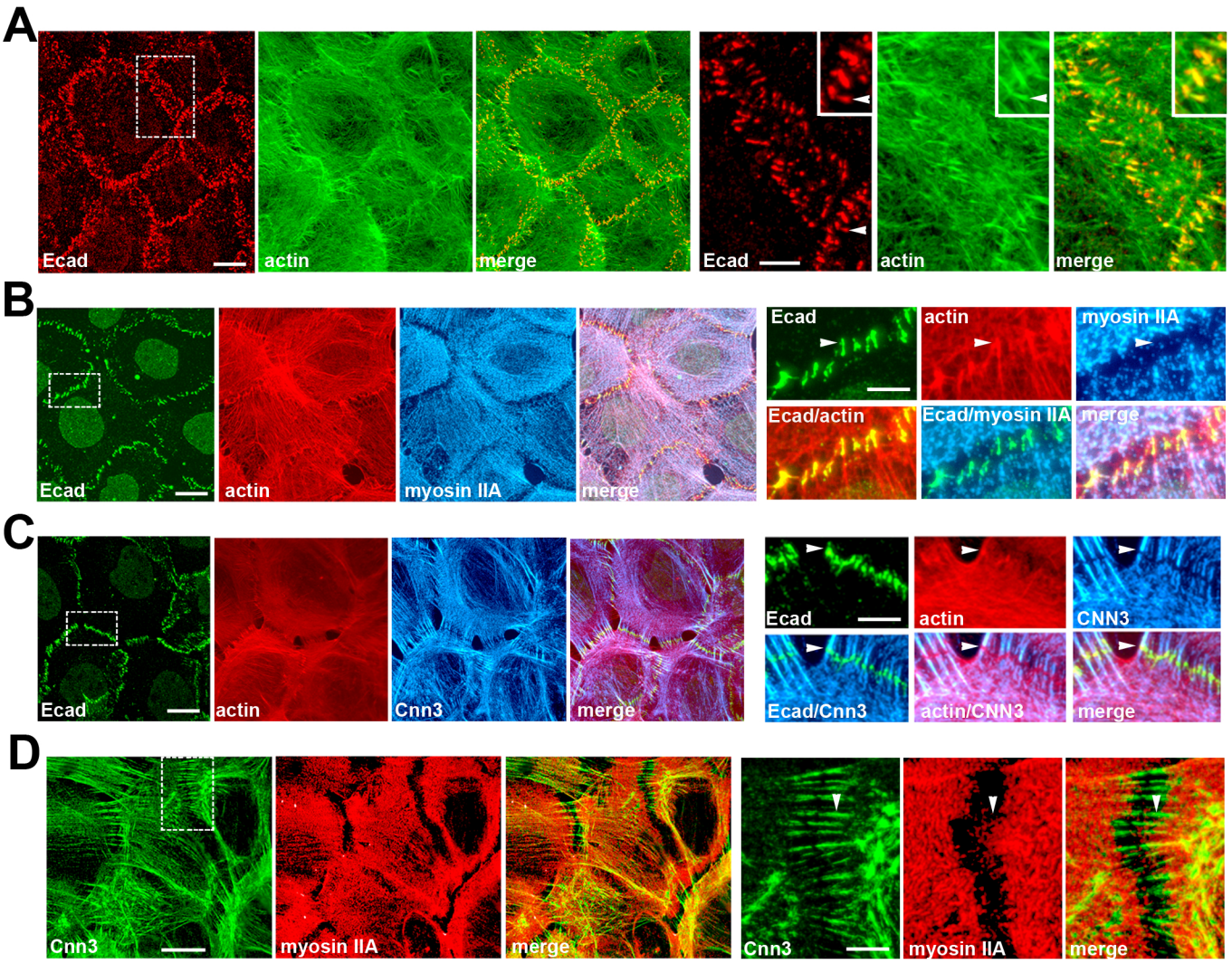
A
Ecad
actin
merge
Ecad
actin
merge
B
Ecad
actin
myosin IIA
merge
Ecad
actin
myosin IIA
Ecad/actin
Ecad/myosin IIA
merge
C
Ecad
actin
Cnn3
merge
Ecad
actin
CNN3
Ecad/Cnn3
actin/CNN3
merge
D
Cnn3
myosin IIA
merge
Cnn3
myosin IIA
merge

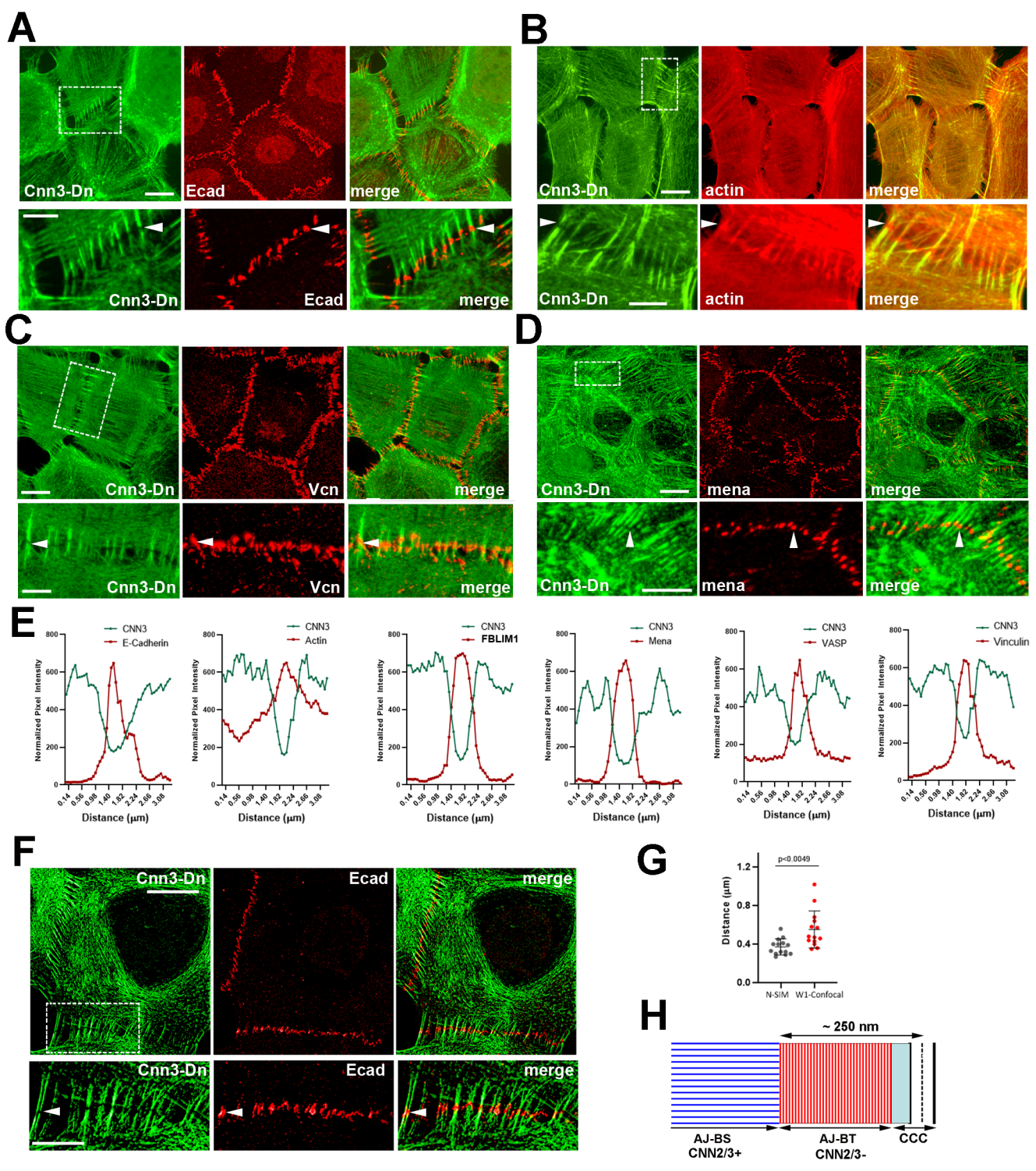
A
Cnn3-Dn
Ecad
merge
Cnn3-Dn
Ecad
merge
B
Cnn3-Dn
actin
merge
Cnn3-Dn
actin
merge
C
Cnn3-Dn
Vcn
merge
Cnn3-Dn
Vcn
merge
D
Cnn3-Dn
mena
merge
Cnn3-Dn
mena
merge
E
CNN3
E-Cadherin
CNN3
Actin
CNN3
FBLIM1
CNN3
Mena
CNN3
VASP
CNN3
Vinculin
Normalized Pixel Intensity
Distance (μm)
F
Cnn3-Dn
Ecad
merge
Cnn3-Dn
Ecad
merge
G
p<0.0049
Distance (μm)
N-SIM
W1-Confocal
H
~ 250 nm
AJ-BS
CNN2/3+
AJ-BT
CNN2/3-
CCC

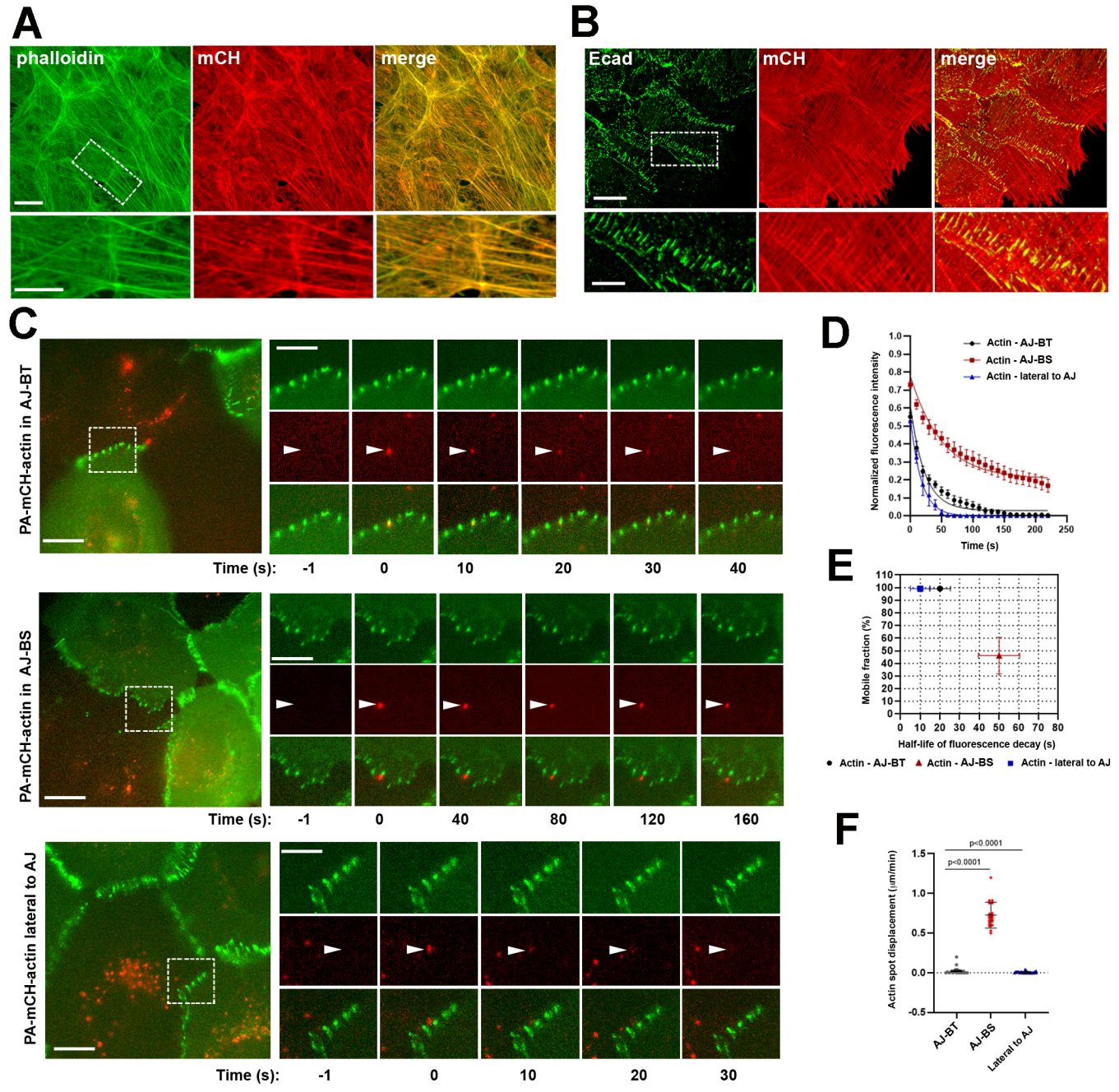
A
phalloidin
mCH
merge
B
Ecad
mCH
merge
C
PA-mCH-actin in AJ-BT
Time (s): -1 0 10 20 30 40
PA-mCH-actin in AJ-BS
Time (s): -1 0 40 80 120 160
PA-mCH-actin lateral to AJ
Time (s): -1 0 10 20 30
D
Actin - AJ-BT
Actin - AJ-BS
Actin - lateral to AJ
Normalized fluorescence intensity
Time (s)
E
Mobile fraction (%)
Half-life of fluorescence decay (s)
Actin - AJ-BT
Actin - AJ-BS
Actin - lateral to AJ
F
Actin spot displacement (µm/min)
p<0.0001
p<0.0001
AJ-BT
AJ-BS
Lateral to AJ

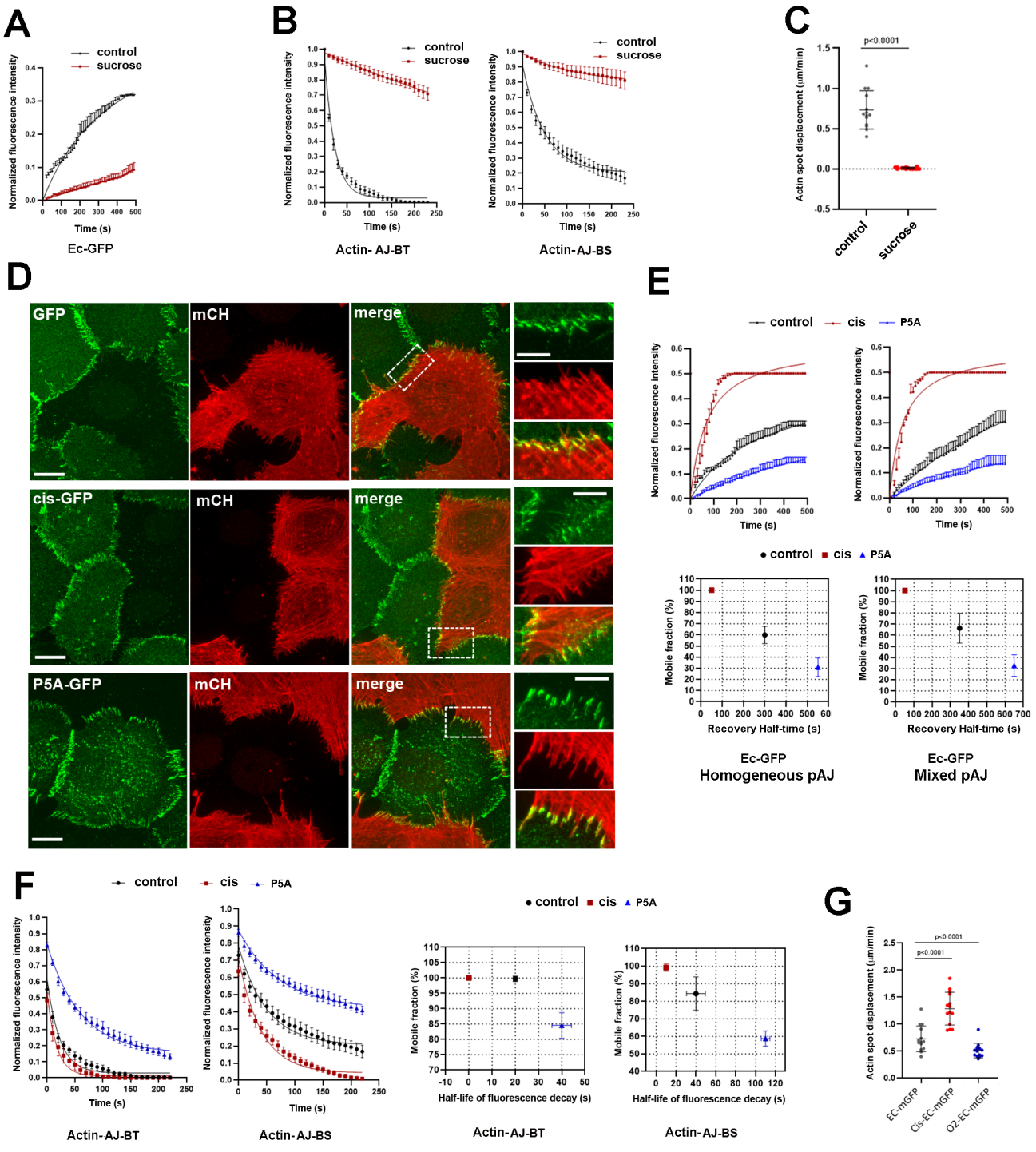
A
control
sucrose
Normalized fluorescence intensity
Time (s)
Ec-GFP
B
control
sucrose
Normalized fluorescence intensity
Time (s)
Actin- AJ-BT
Actin- AJ-BS
C
p<0.0001
Actin spot displacement (µm/min)
control
sucrose
D
GFP
mCH
merge
cis-GFP
P5A-GFP
E
control
cis
P5A
Normalized fluorescence intensity
Time (s)
Mobile fraction (%)
Recovery Half-time (s)
Ec-GFP
Homogeneous pAJ
Ec-GFP
Mixed pAJ
F
Half-life of fluorescence decay (s)
Actin-AJ-BT
Actin-AJ-BS
G
p<0.0001
Actin spot displacement (µm/min)
EC-mGFP
Cis-EC-mGFP
O2-EC-mGFP

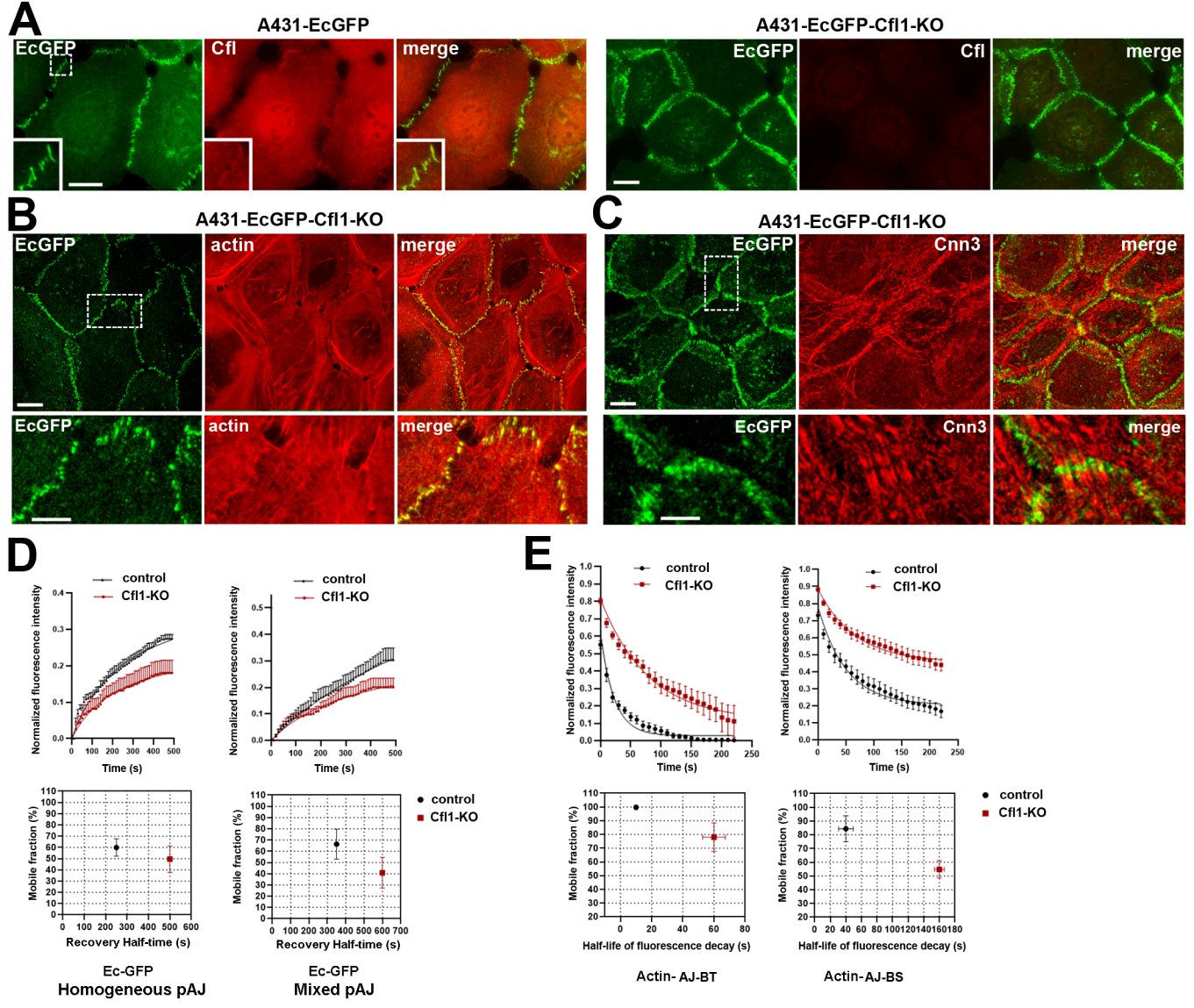
A
A431-EcGFP
EcGFP
Cfl
merge
A431-EcGFP-Cfl1-KO
EcGFP
Cfl
merge
B
A431-EcGFP-Cfl1-KO
EcGFP
actin
merge
EcGFP
actin
merge
C
A431-EcGFP-Cfl1-KO
EcGFP
Cnn3
merge
EcGFP
Cnn3
merge
D
control
Cfl1-KO
Normalized fluorescence intensity
Time (s)
control
Cfl1-KO
Normalized fluorescence intensity
Time (s)
Mobile fraction (%)
Recovery Half-time (s)
Mobile fraction (%)
Recovery Half-time (s)
control
Cfl1-KO
Ec-GFP
Homogeneous pAJ
Ec-GFP
Mixed pAJ
E
control
Cfl1-KO
Normalized fluorescence intensity
Time (s)
control
Cfl1-KO
Normalized fluorescence intensity
Time (s)
Mobile fraction (%)
Half-life of fluorescence decay (s)
Mobile fraction (%)
Half-life of fluorescence decay (s)
control
Cfl1-KO
Actin-AJ-BT
Actin-AJ-BS

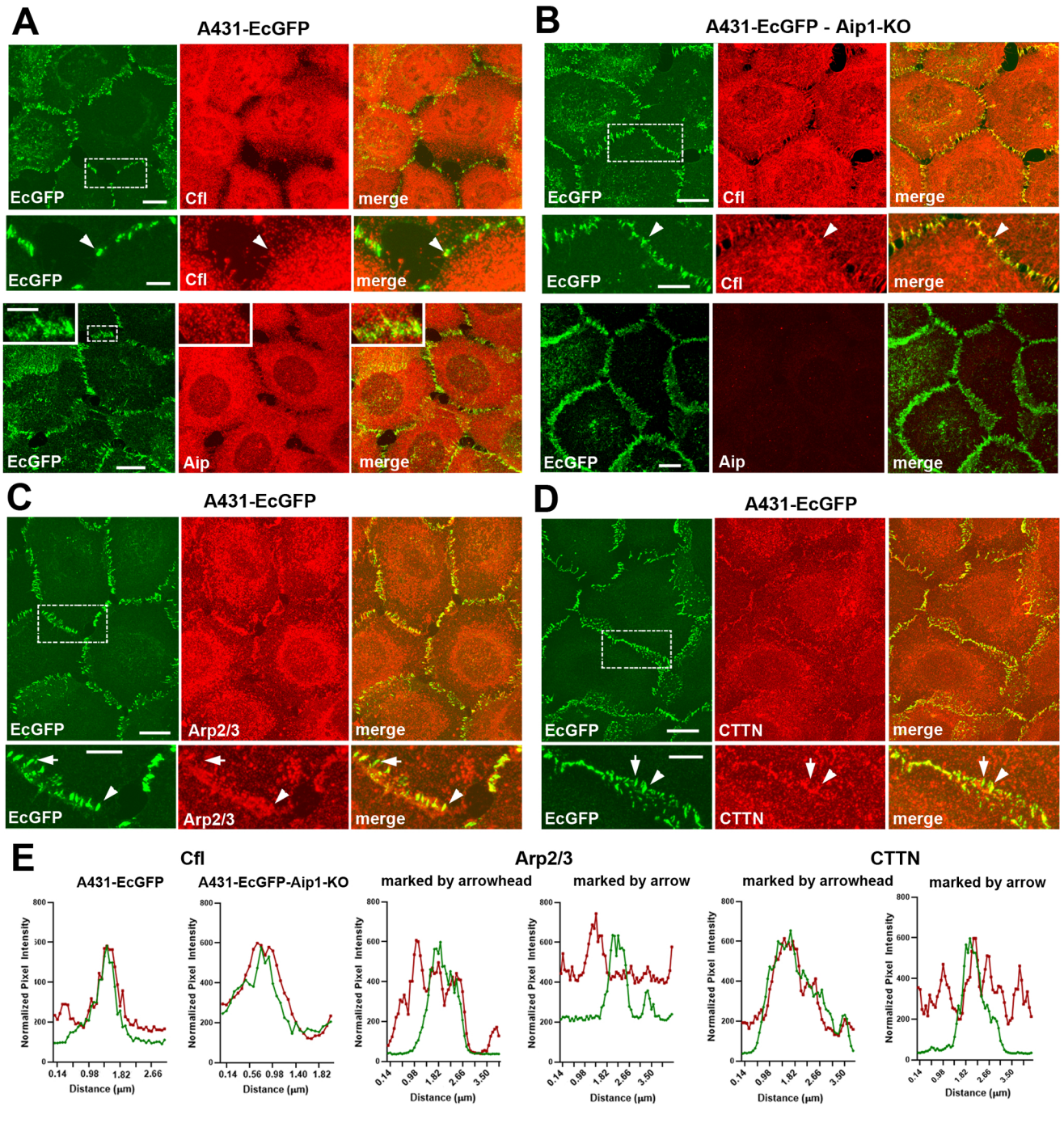
A
A431-EcGFP
EcGFP
Cfl
merge
EcGFP
Cfl
merge
EcGFP
Aip
merge
B
A431-EcGFP - Aip1-KO
EcGFP
Cfl
merge
EcGFP
Cfl
merge
EcGFP
Aip
merge
C
A431-EcGFP
EcGFP
Arp2/3
merge
EcGFP
Arp2/3
merge
D
A431-EcGFP
EcGFP
CTTN
merge
EcGFP
CTTN
merge
E
Cfl
A431-EcGFP
A431-EcGFP-Aip1-KO
Arp2/3
marked by arrowhead
marked by arrow
CTTN
marked by arrowhead
marked by arrow
Normalized Pixel Intensity
Distance (μm)
0.14
0.98
1.82
2.66
0.56
1.40
3.50

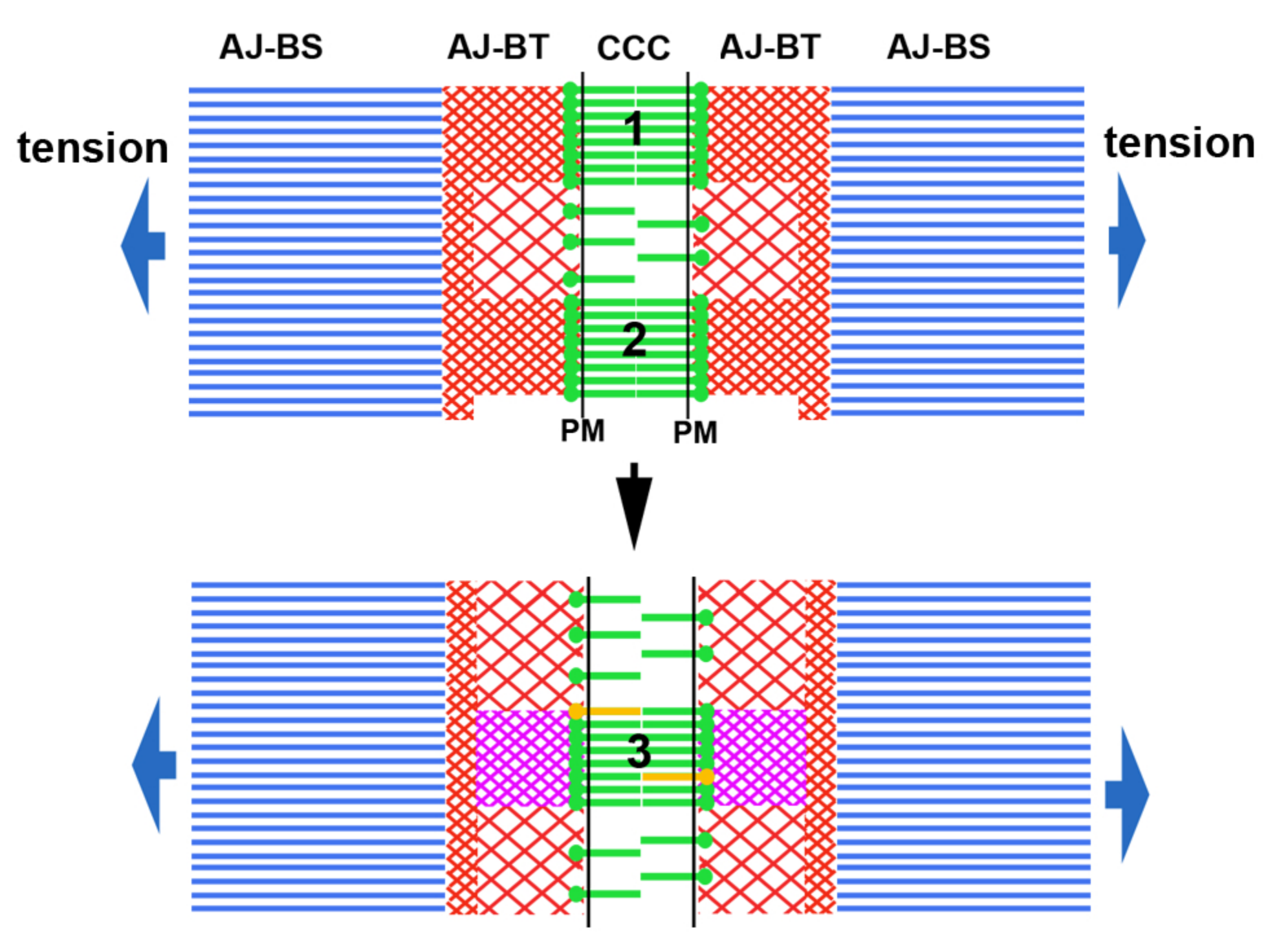
AJ-BS
AJ-BT
CCC
AJ-BT
AJ-BS
tension
tension
1
2
PM
PM
3

STAR METHODS

LEAD CONTACT AND MATERIALS AVAILABILITY

Further information and requests for resources and reagents should be directed to and will be fulfilled by the Lead Contact, Sergey M. Troyanovsky (s-troyanovsky@northwestern.edu). Materials generated in this study are available from the Lead Contact without restrictions.

EXPERIMENTAL MODEL AND SUBJECT DETAILS

Cells and Transfection

A431 cell line used in this study derived from an epidermal carcinoma. Cells were cultured in DMEM supplemented with 10% Fetal Bovine Serum. Transfection and growth of A431 cells and A431-EcKO cells were done as described (Hong et al., 2011; Indra et al., 2018). After transfection and antibiotic selection, the cells were sorted for moderate transgene expression by FACS. Importantly, A431-EcKO version of A431 cells were used for expression of the recombinant E-cadherin or its mutants. The expression of the endogenous E-cadherin in these cells was knocked out by CRISPR-Cas9 approach (Indra et al., 2018). To knockout Cfl1 and Aip1 (the name of corresponding gene is WDR1) in A431-EcGFP cells, the Alt-R^{tm} CRISPR-Cas9 System (IDT, Coralville, IA) was used as it was described previously (Choi et al., 2019). The cells were transfected with an RNA complex consisting of Cfl1-specific or Aip1-specific guide RNAs (5'-tctatgatgcaacctatgag or 5'-ggcgtctccaagatcatcgg designed by software of Broad Institute of Harvard and MIT) and transactivating RNA. The deficient cell clones were then selected through cloning and immunostaining.

METHOD DETAILS

Plasmids

The plasmid encoding E-cadherin and cis-E-cadherin mutant tagged with mGFP and mCH (pRc-EcmGFP and pRcEcmCH) have been reported (Indra et al., 2018). The plasmid containin cis-EcmGFP and P5A-EcmGFP was constructed using pRc-EcmGFP

as a template by site directed mutagenesis and verified by sequencing. The plasmid encoding PA-mCH-tagged b-actin was a gift from Dr. Verkhusha (Addgene, plasmid # 31949). pRc-CNN3-mGFP plasmid was generated by using Myc-DDK tagged CNN3 (Origene, RC200488). In brief, full length CNN3 was PCR amplified by flanking unique restriction sites Nhe1 and Not1 at 5' and 3' sites respectively and inserted between Nhe1/Not1 sites of pRcCMV-Dn vector.

Immunofluorescence Microscopy

For immunofluorescence, cells were fixed with 2% formaldehyde (for 10 min) and permeabilized with 1% Triton X-100 (for 15 min). For Arp2/3 and cortactin staining, the cells were first incubated for 2 min with 1% formaldehyde/0.5%Triton-X-100 in cytoskeleton-preserving buffer (80 mM PIPES pH 6.8, 5 mM EGTA, 2 mM $MgCl_2$) described in (Heuser & Kirschner, 1980) and only then fixed in 2% formaldehyde. In this case the cells were stained without additional permeabilization step. For Cfl staining (Fig. 5A), the cells were fixed by iced-cold methanol (5 min) and then acetone (2 min). For confocal microscopy, the cells were cultured 48-64 h on glass-bottom dishes (P35G-1.5; MatTek) and fixed as described above. Immediately before imaging the dishes were filled with 97% glycerol. The images were taken using Nikon Eclipse Ti2-W1-Spinning Disk Perfect Focus microscope equipped with 100x/1.45 NA Plan Apochromat TIRF lens and Hamamatsu Flash 4.0 CMOS Camera. The images were then processed and analyzed using Nikon's NIS-Element platform version 5.1.

The following antibodies were used: mouse antibodies against E-cadherin (clone HECD1 - Zymed Laboratories, South San Francisco, CA), Cfl1 (clone E-8, Santa Cruz Inc., Dallas, TX), VASP (BD Biosciences, San Jose, CA), vinculin and cortactin (clone hVIN-1 and 4F11, Sigma-Aldrich Co., Saint Louis, MO) and rabbit antibodies against MyoIIA (909801 – Biolegend, San Diego, CA), CNN2 and WDR1 (Aip1) (PA5-61878 and PA5-84836 Invitrogen, Carlsbad, CA), CNN3 (ab204365, Abcam, Cambridge MA), mena and FBLIM1 (NBP1-67914, and NBP2-57310 both from Novus Biologicals, Littleton, CO), mCH (5993, BioVision, Mountain View, CA). Three different rabbit antibodies against Arp2/3 complex were used: against ARPC2 and p16 (ab133315 and ab51243, Abcam) and against ARPC2 (07-227, Millipore, Temecula, CA). Specificity of

all the antibodies, except anti-mCH and anti-Arp2/3 complex, was tested by a combination of Western blotting and specific CRISPR/Cas9 knockout. All three anti-Arp2/3 antibodies yielded the same staining pattern. Secondary antibodies were produced in Donkey (Jackson Immunoresearch Laboratories, West Grove, PA). Alexa Fluor 555-conjugated phalloidin was purchased from Invitrogen.

Live-cell Imaging

Cells were imaged (in L-15 media with 10% FBS) by Eclipse Ti microscope (Nikon, Melville, NY) at 37ºC controlled with Nikon's NIS-Elements software. The microscope was equipped with an incubator chamber, a Prime 95B sCMOS camera (Photometrics), halogen and LED light sources and a Plan Apo TIRF DICN2 100x/1.49 lens. The 1x1 binning mode was used in most imaging experiments. At this microscope setting the pixel size was 110 nm. Time-lapse images were taken in both FITC and mCherry filter sets using halogen light that minimize phototoxicity and photobleaching essentially as described earlier (Chen et al., 2015). The mCH_{PA}-actin located at the point of interest was activated by a 50-ms-long exposure to the 405-nm wavelength laser focused to the diffraction-limited spot (~ 500 nm in diameter). The green and red images were then taken at the indicated intervals (typically 10 sec). For FRAP assay a circular ROI with ~ 500 nm diameter was bleached to approximately 50% of its initial intensity using 40% 405nm laser power.

QUANTIFICATION AND STATISTICAL ANALYSIS

Image Quantifications

All images were saved as nd2 files and processed using NIS-Element v5.0 (Nikon) or ImageJ softwares (National Institutes of Health). Line-scan analysis (Figs. 2E and 6E) was done using NIS-Element v5.0. Time-lapse images were processed using limited background reduction and denoising functions of NIS-Element. In FRAP and FLIP experiments, the fluorescence intensity of each region was first adjusted by subtracting the background intensity and then normalized to the intensity at the initial time point using NIS Element 5.0. Both red and green channels were treated equally.

A single square-size "ROI" was created covering the point of fluorescence bleaching or conversion using ImageJ. The recovery or reduction of fluorescence of the selected ROI was recorded for the entire time lapse images using ImageJ. All graphs, chards and error bars were plotted using GraphPad Prism 8. Fluorescence recovery curves of FRAP analysis (Figs. 4A,E, 5D, and S2) were fitted using Michaelis-Menten equation (Y=Vmax*X/(Km+X)) and Fluorescence loss in photo-activation curves of FLIP analysis (Figs. 3D, 4B,F, 5E) were fitted using one phase exponential decay (Y=(Y0-NS)*exp(-K*X) + NS). All data were represented as the mean ± standard error of the mean (SEM). All n-values per group are reported in the figure legends. Statistical significance was analyzed using the Student's two-tailed t test for two groups and ANOVA analysis for more groups. A p value that was less than 0.05 was considered statistically significant.

DATA AND CODE AVAILABILITY

This study did not generate/analyze datasets of codes.

Supplemental video

Movie S1. High instability of the AJ-BT actin. Related to Figure 3C. "Dark" A431 cells expressing mCH_{PA}-actin were co-cultured with EcGFP-expressing cells. Actin was photoactivated in a diffraction-limited spot (~ 500 nm in diameter) precisely in the selected EcGFP-tagged pAJ. The movie frames (in 10 sec intervals) were taken in green and red imaging channels: green channel detects EcGFP, while red channel detects only background fluorescence before and red fluorescence of mCH_{PA}-actin after photoactivation. Note that the photoactivated spot is stationary and aligned with the selected pAJ (see Fig. 3 for detail).

Movie S2. AJ-BS actin displays centripetal movement. Related to Figure 3C. mCH_{PA}-actin was photoactivated exactly as in Movie S1 but 0.5 μm away from EcGFP-tagged pAJ. Note that the photoactivated spot is much more stable then in Movie 1 and motile (see Fig. 3 for detail).

Movie S3. High instability of the interjunctional actin. Related to Figure 3C. The spot of mCH$_{PA}$-actin was photoactivated exactly as in Movie S1 but between two EcGFP-tagged pAJs (see Fig. 3 for detail).

DECLARATION OF INTERESTS

The authors declare no competing interests.

References

Abe, H., Nagaoka, R., and Obinata, T. (1993). Cytoplasmic localization and nuclear transport of cofilin in cultured myotubes. Exp Cell Res. 206, 1-10.

Bravo-Cordero, J.J., Magalhaes, M.A., Eddy, R.J., Hodgson, L., and Condeelis, J. (2013). Functions of cofilin in cell locomotion and invasion. Nat Rev Mol Cell Biol. 14, 405-415

Brieher, W.M., and Yap, A.S. (2013). Cadherin junctions and their cytoskeleton(s). Curr Opin Cell Biol. 25, 39-46.

Buckley, C.D., Tan, J., Anderson, K.L., Hanein, D., Volkmann, N., Weis, W.I., Nelson, W.J., and Dunn, A.R. (2014). Cell adhesion. The minimal cadherin-catenin complex binds to actin filaments under force. Science. 346, 1254211.

Cavey, M., Rauzi, M., Lenne, P.F., and Lecuit, T. (2008). A two-tiered mechanism for stabilization and immobilization of E-cadherin. Nature. 453, 751-756.

Case, L.B., and Waterman, C.M. (2015). Integration of actin dynamics and cell adhesion by a three-dimensional, mechanosensitive molecular clutch. Nat Cell Biol. 17, 955-963.

Changede, R., and Sheetz, M. (2017). Integrin and cadherin clusters: A robust way to organize adhesions for cell mechanics. Bioessays. 39, 1-12.

Chu, D., Pan, H., Wan, P., Wu, J., Luo, J., Zhu, H., and Chen, J. (2012). AIP1 acts with cofilin to control actin dynamics during epithelial morphogenesis. Development. 139, 3561-3571.

Ciuba, K., Hawkes, W., Tojkander, S., Kogan, K., Engel, U., Iskratsch, T., and Lappalainen, P. (2018). Calponin-3 is critical for coordinated contractility of actin stress fibers. Sci Rep. 8, 17670.

Chan, C., Beltzner, C.C., and Pollard, T.D. (2009). Cofilin dissociates Arp2/3 complex and branches from actin filaments. Curr Biol. 19, 537-545.

Chen, C.S., Hong, S., Indra, I., Sergeeva, A.P., Troyanovsky, R.B., Shapiro, L., Honig, B., and Troyanovsky, S.M. 2015. α-Catenin-mediated cadherin clustering couples cadherin and actin dynamics. J Cell Biol. 210, 647-661.

Choi, W., Acharya, B.R., Peyret, G., Fardin, M.A., Mège, R.M., Ladoux, B., Yap, A.S., Fanning, A.S., and Peifer, M. (2016). Remodeling the zonula adherens in response to tension and the role of afadin in this response. J Cell Biol. 213, 243-260.

Choi, J., Troyanovsky, R.B., Indra, I., Mitchell, B.J., and Troyanovsky, S.M. (2019). Scribble, Erbin, and Lano redundantly regulate epithelial polarity and apical adhesion complex. J Cell Biol. 218, 2277-2293.

de Beco, S., Perney, J.B., Coscoy, S., and Amblard, F. (2015). Mechanosensitive Adaptation of E-Cadherin Turnover across adherens Junctions. PLoS One. 10:e0128281

Efimova, N., and Svitkina, T.M. (2018). Branched actin networks push against each other at adherens junctions to maintain cell-cell adhesion. J Cell Biol. 217, 1827-1845.

Fritzsche, M., Lewalle, A., Duke, T., Kruse, K., and Charras, G. (2013). Analysis of turnover dynamics of the submembranous actin cortex. Mol Biol Cell. 24, 757-767.

Geiger, B., Spatz, J.P., and Bershadsky, A.D. (2009). Environmental sensing through focal adhesions. Nat Rev Mol Cell Biol. 10, 21-33.

Guo, Z., Neilson, L.J., Zhong, H., Murray, P.S., Zanivan, S., and Zaidel-Bar, R. (2014). E-cadherin interactome complexity and robustness resolved by quantitative proteomics. Sci Signal. 7, rs7.

Han, S.P., Gambin, Y., Gomez, G.A., Verma, S., Giles, N., Michael, M., Wu, S.K., Guo, Z., Johnston, W., Sierecki, et al. (2014). Cortactin scaffolds Arp2/3 and WAVE2 at the epithelial zonula adherens. J Biol Chem. 289, 7764-7775.

Hansen, S.D., Kwiatkowski, A.V., Ouyang, C.Y., Liu, H., Pokutta, S., Watkins, S.C., Volkmann, N., Hanein, D., Weis, W.I., Mullins, R.D., and Nelson, W.J. (2013). αE-catenin actin-binding domain alters actin filament conformation and regulates binding of nucleation and disassembly factors. Mol Biol Cell. 24, 3710-3720.

Harris, T.J., and Tepass, U. (2010). Adherens junctions: from molecules to morphogenesis. Nat Rev Mol Cell Biol. 11, 502-514.

Harrison, O.J., Jin, X., Hong, S., Bahna, F., Ahlsen, G., Brasch, J., Wu, Y., Vendome, J., Felsovalyi, K., Hampton, C.M., Troyanovsky, R.B. et al. (2011). The extracellular architecture of adherens junctions revealed by crystal structures of type I cadherins. Structure. 19, 244-256.

Heuser, J.E. and Kirschner, M.W. (1980). Filament organization revealed in platinum replicas of freeze-dried cytoskeletons. J. Cell Biol. 86, 212-234.

Hong, S., Troyanovsky, R.B., and Troyanovsky, S.M. (2011). Cadherin exits the junction by switching its adhesive bond. J Cell Biol. 192, 1073-1083.

Hotulainen, P., Paunola, E., Vartiainen, M.K., and Lappalainen, P. (2005). Actin-depolymerizing factor and cofilin-1 play overlapping roles in promoting rapid F-actin depolymerization in mammalian nonmuscle cells. Mol Biol Cell. 16, 649-664.

Hotulainen, P., and Lappalainen, P. (2006). Stress fibers are generated by two distinct actin assembly mechanisms in motile cells. J Cell Biol. 173, 383-394.

Huveneers, S., and de Rooij, J. (2013). Mechanosensitive systems at the cadherin-F-actin interface. J Cell Sci. 126, 403-413.

Indra, I., Hong, S., Troyanovsky, R., Kormos, B., Troyanovsky, S. (2013). The adherens junction: a mosaic of cadherin and nectin clusters bundled by actin filaments. J Invest Dermatol. 133, 2546-2554.

Indra, I., Choi, J., Chen, C.S., Troyanovsky, R.B., Shapiro, L., Honig, B., and Troyanovsky, S.M. (2018). Spatial and temporal organization of cadherin in punctate adherens junctions. Proc Natl Acad Sci U S A. 115, E4406-E4415.

Iwasa, J.H., and Mullins, R.D. (2007). Spatial and temporal relationships between actin-filament nucleation, capping, and disassembly. Curr Biol. 17, 395-406.

Kato, A., Kurita, S., Hayashi, A., Kaji, N., Ohashi, K., and Mizuno, K. (2008). Critical roles of actin-interacting protein 1 in cytokinesis and chemotactic migration of mammalian cells. Biochem J. 414, 261-270.

Kovacs, E.M., Goodwin, M., Ali, R.G., Paterson, A.D., and Yap, A.S. (2002). Cadherin-directed actin assembly: E-cadherin physically associates with the Arp2/3 complex to direct actin assembly in nascent adhesive contacts. Curr Biol. 12, 379-382.

Kovacs EM, Verma S, Ali RG, Ratheesh A, Hamilton NA, Akhmanova A, Yap AS. (2011). N-WASP regulates the epithelial junctional actin cytoskeleton through a non-canonical post-nucleation pathway. Nat Cell Biol. 13:934-943.

Lai, F.P., Szczodrak, M., Block, J., Faix, J., Breitsprecher, D., Mannherz, H.G., Stradal, T.E., Dunn, G.A., Small, J.V., and Rottner, K. (2008). Arp2/3 complex interactions and actin network turnover in lamellipodia. EMBO J. 27, 982-92.

Lappalainen, P., and Drubin, D.G. (1997). Cofilin promotes rapid actin filament turnover in vivo. Nature. 388, 78–82.

Lee, N.K., Fok, K.W., White, A., Wilson, N.H., O'Leary, C.J., Cox, H.L., Michae,l M., Yap, A.S., Cooper, H.M. (2016). Neogenin recruitment of the WAVE regulatory complex maintains adherens junction stability and tension. Nat Commun. 7, 11082.

Leerberg, J.M., Gomez, G.A., Verma, S., Moussa, E.J., Wu, S.K., Priya, R., Hoffman, B.D., Grashoff, C., Schwartz, M.A., and Yap, A.S. (2014). Tension-sensitive actin assembly supports contractility at the epithelial zonula adherens. Curr Biol. 24, 1689-1699.

Li, Y., Merkel, C.D., Zeng, X., Heier, J.A., Cantrell, P.S., Sun, M., Stolz, D.B., Watkins, S.C., Yates, N.A., and Kwiatkowski, A.V. (2019). The N-cadherin interactome in primary cardiomyocytes as defined using quantitative proximity proteomics. J Cell Sci. 132(3). pii: jcs221606

Michael, M., and Yap, A.S. (2013). The regulation and functional impact of actin assembly at cadherin cell-cell adhesions. Semin Cell Dev Biol. 24, 298-307.

Mège, R.M., and Ishiyama, N. (2017). Integration of Cadherin Adhesion and Cytoskeleton at Adherens Junctions. Cold Spring Harb Perspect Biol. 9 pii: a028738.

Munsie, L.N, Desmond, C.R., and Truant, R. (2012). Cofilin nuclear-cytoplasmic shuttling affects cofilin-actin rod formation during stress. J Cell Sci. 125, 3977-3988.

Pappas, D.J., and Rimm DL. (2006). Direct interaction of the C-terminal domain of alpha-catenin and F-actin is necessary for stabilized cell-cell adhesion. Cell Commun Adhes. 13, 151-170.

Scott, J.A., Shewan, A.M., den Elzen, N.R., Loureiro, J.J., Gertler, F.B., and Yap, A.S. (2006). Ena/VASP proteins can regulate distinct modes of actin organization at cadherin-adhesive contacts. Mol Biol Cell. 17, 1085-95.

Strale, P.O., Duchesne, L., Peyret, G., Montel, L., Nguyen, T., Png, E., Tampé, R., Troyanovsky, S., Hénon, S., Ladoux, B., and Mège, R.M. (2015). The formation of ordered nanoclusters controls cadherin anchoring to actin and cell-cell contact fluidity. J Cell Biol. 210, 333-346.

Subach, F.V., Patterson, G.H., Manley, S., Gillette, J.M., Lippincott-Schwartz, J., and Verkhusha, V.V. (2009). Photoactivatable mCherry for high-resolution two-color fluorescence microscopy. Nat Methods. 6,153-159

Tang, V.W., and Brieher, W.M. (2012). α-Actinin-4/FSGS1 is required for Arp2/3-dependent actin assembly at the adherens junction. J Cell Biol. 196, 115-130.

Tojkander, S., Gateva, G., and Lappalainen, P. (2012). Actin stress fibers-assembly, dynamics and biological roles. J Cell Sci. 125, 1855-1864.

Tojkander, S., Gateva, G., Husain, A., Krishnan, R., and Lappalainen, P. (2015). Generation of contractile actomyosin bundles depends on mechanosensitive actin filament assembly and disassembly. Elife. 4, e06126.

Troyanovsky, R.B., Sokolov, E.P., and Troyanovsky, S.M. (2006). Endocytosis of cadherin from intracellular junctions is the driving force for cadherin adhesive dimer disassembly. Mol Biol Cell. 17, 3484-3493.

Van Itallie, C.M., Tietgens, A.J., Aponte, A., Fredriksson, K., Fanning, A.S., Gucek, M., and Anderson, J.M. (2014). Biotin ligase tagging identifies proteins proximal to E-cadherin, including lipoma preferred partner, a regulator of epithelial cell-cell and cell-substrate adhesion. J Cell Sci. 127, 885-895.

Vasioukhin, V., Bauer, C., Yin, M., and Fuchs, E. (2000). Directed actin polymerization is the driving force for epithelial cell-cell adhesion. Cell. 100, 209-219.

Vendome, J., Posy, S., Jin, X., Bahna, F., Ahlsen, G., Shapiro, L., and Honig, B. (2011). Molecular design principles underlying β-strand swapping in the adhesive dimerization of cadherins. Nat Struct Mol Biol. 18, 693-700.

Verma, S., Shewan, A.M., Scott, J.A., Helwani, F.M., den Elzen, N.R., Miki, H., Takenawa, T., and Yap, A.S. (2004). Arp2/3 activity is necessary for efficient formation of E-cadherin adhesive contacts. J Biol Chem. 279, 34062-34070

Vitriol, E.A., Wise, A.L., Berginski, M.E., Bamburg, J.R., and Zheng, J.Q. (2013). Instantaneous inactivation of cofilin reveals its function of F-actin disassembly in lamellipodia. Mol Biol Cell. 24, 2238-2247.

Wang, D., Naydenov, N.G., Feygin, A., Baranwal, S., Kuemmerle, J.F., and Ivanov, A.I. (2016). Actin-Depolymerizing Factor and Cofilin-1 Have Unique and Overlapping Functions in Regulating Intestinal Epithelial Junctions and Mucosal Inflammation. Am J Pathol. 186, 844-858.

Yamada, S., Pokutta, S., Drees, F., Weis, W.I., and Nelson W. J. (2005). Deconstructing the cadherin-catenin-actin complex. Cell. 123, 889-901.

Yonemura, S., Itoh, M., Nagafuchi, A., and Tsukita, S. (1995). Cell-to-cell adherens junction formation and actin filament organization: similarities and differences between non-polarized fibroblasts and polarized epithelial cells. J Cell Sci. 108, 127-142.

Zhang, J., Betson, M., Erasmus, J., Zeikos, K., Bailly, M., Cramer, L.P., and Braga, V.M. (2005). Actin at cell-cell junctions is composed of two dynamic and functional populations. J Cell Sci. 118, 5549-5562.

Yap, A.S., Duszyc, K., and Viasnoff, V. 2018. Mechanosensing and Mechanotransduction at Cell-Cell Junctions. Cold Spring Harb Perspect Biol. 10, a028761.

KEY RESOURCES TABLE

REAGENT or RESOURCE	SOURCE	IDENTIFIER
Antibodies		
E-cadherin (mouse, monoclonal, clone HECD1)_	Millipore	Cat# 205601; RRID:AB_211510
Cfl1 (mouse, monoclonal, clone E-8)	Santa Cruz Biotechnology	Cat# sc-376476, RRID: AB_11150468
VASP (mouse monoclonal, clone 43)	BD Biosciences	Cat# 610447, RRID:AB_397821
Vinculin (mouse, clone hVIN-1)	Sigma-Aldrich	Cat# V9131, RRID:AB_477629
Cortactin (mouse monoclonal, clone 4F11)	Millipore	Cat# 05-180, RRID:AB_309647
MyoIIA (rabbit polyclonal)	BioLegend	Cat# 909801, RRID:AB_2565100
Calponin-2 (rabbit polyclonal)	Thermo Fisher Scientific	Cat# PA5-61878, RRID:AB_2639249
WDR1 (Aip1) (rabbit polyclonal)	Thermo Fisher Scientific	Cat# PA5-84836, RRID:AB_2791985
Calponin-3 (rabbit polyclonal)	Abcam	Cat# ab204365
Mena (rabbit polyclonal)	Novus	Cat# NBP1-87914, RRID:AB_11017241
Migfilin (FBLIM1) (rabbit polyclonal)	novus	NBP2-57310
mCherry (rabbit polyclonal)	BioVision	Cat# 5993-100, RRID:AB_1975001
ARPC2 (rabbit monoclonal)	Abcam	Cat# ab133315
P16 ARC (rabbit monoclonal)	Abcam	Cat# ab51243, RRID:AB_2059963
ARPC2 (rabbit polyclonal)	Millipore	Cat# 07-227, RRID:AB_11212539
Alexa Fluor 488-Donkey anti-Mouse IgG	Jackson ImmunoResearch Labs	Cat# 715-545-150, RRID:AB_2340846
Cy3-Donkey anti-Mouse IgG	Jackson ImmunoResearch Labs	Cat# 715-165-150, RRID:AB_2340813
Alexa Fluor 488 Donkey anti-Rabbit IgG	Jackson ImmunoResearch Labs	Cat# 711-545-152, RRID:AB_2313584
Cy3-Donkey anti-Rabbit IgG	Jackson ImmunoResearch Labs	Labs Cat# 711-165-152, RRID:AB_2307443
Chemicals, Peptides, and Recombinant Proteins		
Phalloidin conjugated with Alexa 555	Thermo Fisher Scientific	A34055
Critical Commercial Assays		
CRISPR-Cas9	Alt-R^{tm} CRISPR-Cas9	IDT
Experimental Models: Cell Lines		

A431	German Cancer Research Center (Heidelberg, FRG)	N/A
A431-EcKO	Indra et al., 2018	N/A
A431-Cnn3-Dn	This paper	N/A
A431-EcGFP	Indra et al., 2018	N/A
A431-EcmCH	Indra et al., 2018	N/A
A431-cis-EcGFP	This paper	N/A
A431-P5-AEcGFP	This paper	N/A
A431-EcGFP-Cfl1-KO	This paper	N/A
A431-EcGFP-Aip1-KO	This paper	N/A
Oligonucleotides		
transactivating RNA:	IDT	Cat #
Aip1-specific guide RNAs: 5'-ggcgtctccaagatcatcgg	IDT	N/A
Cfl1-specific guide RNAs: 5’-tctatgatgcaacctatgag	IDT	N/A
Recombinant DNA		
PA-mCH	Subach et al., 2009	Addgene plasmid #31949
pCMVCNN3-Myc	OriGene	RC200488
pRc-EcmGFP	Indra et al., 2018	N/A
pRcEcmCH	Indra et al., 2018	N/A
pRc-CNN3-mGFP	This paper	N/A
pRc-P5A-EcmGFP	This paper	N/A
pRc-cis-EcmGFP	This paper	N/A
Software and Algorithms		
NIS-Element 5.0	Nikon	Nikon
Prism 8	GraphPad	GraphPad
Fiji	IamgeJ	https://imagej.nih.gov/ij/
GPP sgRNA Designer	BROAD Institute GPP Web Portal	https://portals.broadinstitute.org/gpp/public/analysis-tools/sgrna-design

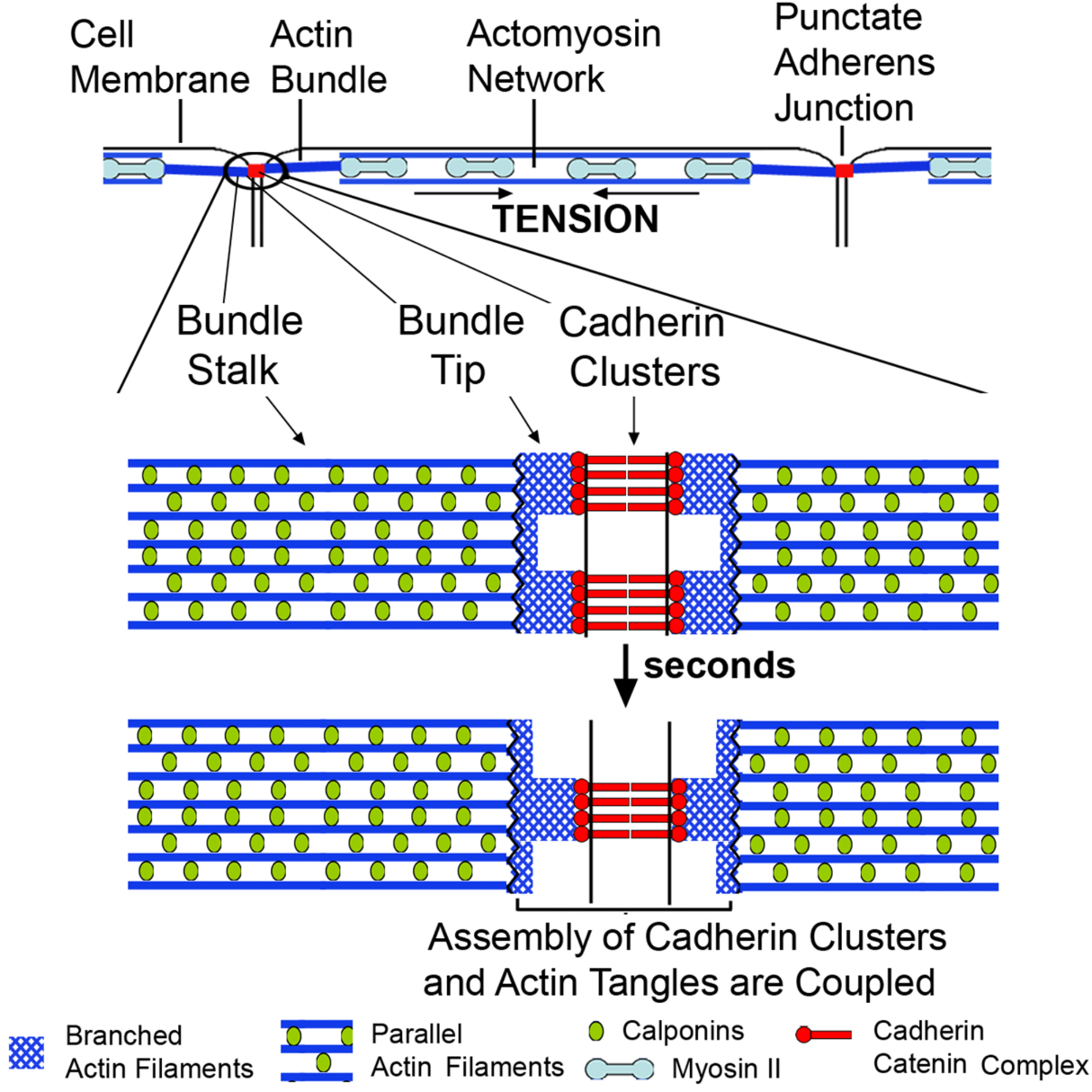
Cell Membrane
Actin Bundle
Actomyosin Network
Punctate Adherens Junction
TENSION
Bundle Stalk
Bundle Tip
Cadherin Clusters
seconds
Assembly of Cadherin Clusters and Actin Tangles are Coupled
Branched Actin Filaments
Parallel Actin Filaments
Calponins
Myosin II
Cadherin Catenin Complex